Variation in acoustic radiation of a fluid-loaded cantilever excited by point or distributed force

R. M. Howell (1)*, W. Waldman (1,2), K. Tsigklifis (1), H. Cao (3), P. Dylejko (1), P. Williams (3) and M. Karimi (3)

(1) Platform Division, Defence Science and Technology, Melbourne, VIC 3207
(2) YTEK Pty Ltd, Level 1, 231 High St, Ashburton, VIC 3147
(3) Centre for Audio, Acoustics and Vibration, University of Technology Sydney, NSW
*Email: richard.howell2@defence.gov.au

Abstract - The acoustic radiation of vibrating fluid-loaded cantilevers is a canonical problem that has many applications in industry e.g. the noise generation of wind-turbine blades. The focus of this study is the extent to which our reduced-order model (Tsigklifis et al., 2022) can capture the underlying physics of this problem that includes the effect of material flexibility on sound generation. An additional benefit is that models of this type are computationally efficient compared to commercial software. Benchmark results for comparison of a fluid-loaded (stationary flow) cantilever are produced using COMSOL. Cantilevers of both uniform and aerofoil cross-section have been excited by point and distributed forces at different locations on the cantilever for frequencies up to 60 kHz generating values of drive-point mobility and acoustic radiation. Of principal interest is the effect of varying the location of the excitation force on the cantilever between the mid-chord and the trailing edge. Our reduced-order model couples a 1D Euler-Bernoulli beam in translation and rotation with Theodorsen's unsteady aerofoil model capturing the added mass and the Rayleigh integral equation for the acoustic radiation. The effect of chordwise modes along the cantilever cannot be modelled using this technique. Their effect is investigated using the fluid-loaded thin plate model of Cao et al. (2023). Initial results show that the dominant features of the COMSOL predictions are well captured by the 1D model for the first three modes of vibration. The 2D model more accurately captures certain features of the high frequency response.

1 INTRODUCTION

The vibroacoustics of fluid-loaded cantilevers is a canonical problem that has many applications in industry e.g. the noise generation of wind-turbine blades. Our previous investigations have examined the fundamental physics through numerical and analytical modelling of sub-problems of the full system. Peters et al. (2014) showed how cantilever natural-frequencies of vibration are modified in axial fluid-flow to enable better prediction of vortex-induced vibration (VIV). Chen and Kessissoglou (2014) demonstrated the effect of material flexibility on the acoustic radiation of trailing-edge noise using the semi-empirical model of Howe (1993). The focus of this study is the extent to which our reduced-order model (ROM) of a fluid-loaded cantilever (Tsigklifis et al., 2022) can capture the effect of material flexibility on acoustic radiation. The ROM couples a 1D beam in bending with a 1D beam in torsion and hence cannot model chordwise modes, an approximation that is known to be effective for lower-order modes of vibration. This study will focus on an aluminium cantilever in water for the simplest case of a static fluid, with a future investigation to examine the effect of a flowing fluid e.g. the effect on trailing-edge noise of an industrial fan (Howell et al., 2022). COMSOL was used to produce benchmark results of drive-point mobility (DPM) and acoustic radiation as the open literature does not contain any substantive experimental data for quantitative validation.

The cantilever geometry is shown in Figure 1 of span $L = 0.08$ m. A uniform cross-section can be modelled with chord length $c_L = 0.05$ m and thickness ratio $h/c_L = 0.15$ and also a tapered cantilever with aerofoil NACA0015 cross-section with the free-end dimensions 50% of the clamp c_L and h. The dimensions are chosen to be similar

to a typical hydrofoil tested in a water tunnel e.g. see Smith et al. (2021).To excite the structure, a linear force F is applied either as a point load at $0.625L$ of magnitude $1\ \mathrm{N}$ at the mid-chord (MC), quarter chord (QC – towards the leading edge) or trailing edge (TE) or apply a uniformly distributed-load along the entire TE with the total applied-force $F = 1\ \mathrm{N}$. Thus the ability of the ROM to capture the effect of point and distributed loads will be demonstrated. To illustrate what increase in accuracy can be gained by including chordwise modes, further results are generated using the fluid-loaded, thin-plate model of Cao et al. (2023).

2 METHODS

We first present a brief overview of the computational methods used in this study with reference to the publications that describe them in full detail.

2.1 COMSOL

The COMSOL Multiphysics commercial code has been used to produce benchmark DPM and acoustic radiation characteristics of the 3D fluid-loaded cantilever. The structural equations are obtained using the finite-element method (FEM), which are then coupled to the acoustic boundary-element method (BEM) in order to solve the fully-coupled equations, with couplings in both directions. The resulting problem is solved with an iterative solver that uses a hybrid preconditioner to handle the FEM part of the matrix and the BEM part of the matrix separately. Serendipity quadratic-elements were used, which include mid-side nodes. A more refined mesh was defined towards the sharp trailing edge of the hydrofoil, with a view to adequately representing modal structural deformations in that lower thickness region: these deformations dominate the higher-frequency mode shapes. With regard to convergence, the acoustic computations make use of at least six panels per-wavelength at $60\ \mathrm{kHz}$ in water. With the 50% taper the panel spacing is even more refined than that in the chordwise direction. The FEM mesh for the hydrofoil displays reasonable *in vacuo* mode shapes at $100\ \mathrm{kHz}$, and the difference in eigenfrequencies is $\sim 1\%$ with double the number of elements. A standard desktop PC typically takes 24 hours to solve a single geometry with all the different load cases: MC, QC and TE for point load and TE distributed load.

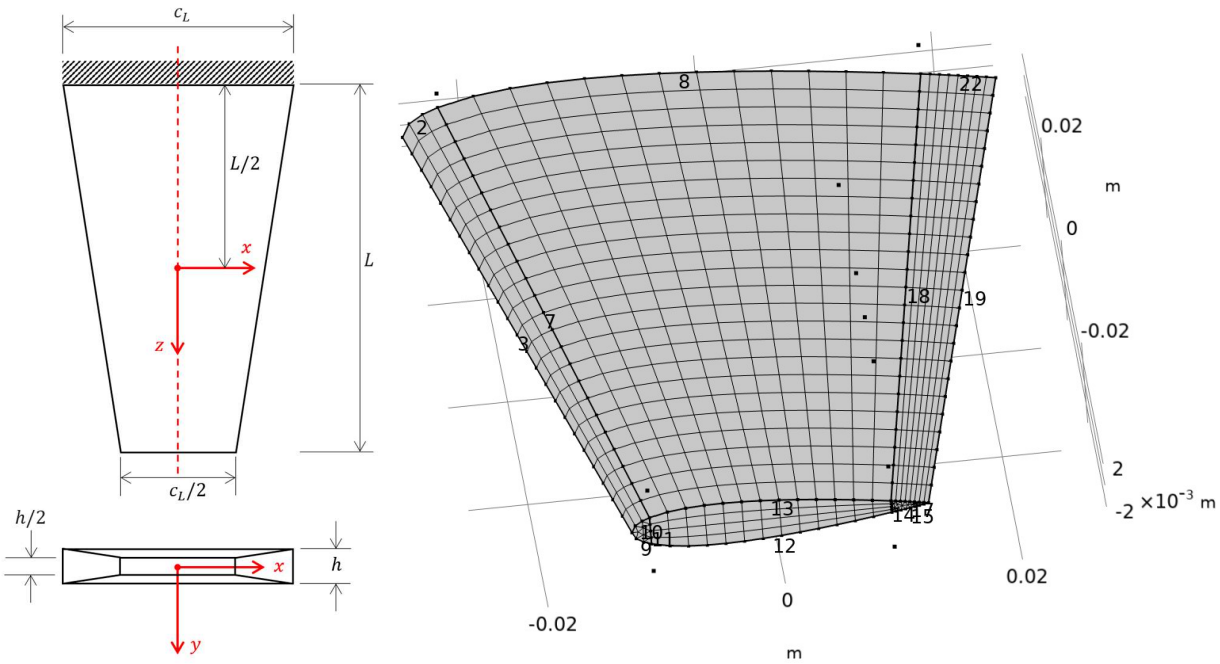

Figure 1 – Left: Geometry of the 50%-tapered cantilever plate with rectangular cross-section. Right: Finite element mesh used in the COMSOL computations for the 50%-tapered NACA0015 cantilevered hydrofoil.

2.2 Reduced-Order Model (ROM)

The dynamic equations of the cantilever hydrofoil-response have been developed in previous work (Tsigklifis et al., 2021, Tsigklifis et al., 2022, Wong et al., 2022, Tsigklifis et al., 2024) and may be written compactly as

$$\boldsymbol{\mathcal{D}}(\eta, z, f)\hat{\boldsymbol{x}} = \boldsymbol{L_G}\left(GRF, \varphi_{u_y u_y}, z, f\right) + \boldsymbol{L_{HP}}(T(\sigma), M_c, z, f)\hat{\boldsymbol{x}}\,. \tag{1}$$

In Equation 1, the left-hand side represents the structural response and right-hand side the forces exerted by the interactions with the hydrodynamic flow. The operator $\mathcal{D}$ describes the bending and torsional motion of the foil, while $\hat{\boldsymbol{x}}$ describes the resultant vertical $\hat{h}$ and angular $\hat{\phi}$ displacements (see Figure 2). Using 2D hydrofoil theory, the unsteady lift and moment response of a hydrofoil section may be described by superimposing two forcing functions $\boldsymbol{L_G}$ and $\boldsymbol{L_{HP}}\hat{\boldsymbol{x}}$. The function $\boldsymbol{L_G}$ arises from the leading edge (LE) of a rigid hydrofoil interacting with an incoming upwash gust and is described by an appropriate gust-response function (GRF) and a turbulence wavenumber-spectrum $\varphi_{u_y u_y}$. The function $\boldsymbol{L_{HP}}\hat{\boldsymbol{x}}$, using Theordorsen's function $T(\sigma)$ at reduced frequency σ, captures the fluid forces due to the heaving (bending) and pitching (torsional) motion of the hydrofoil section that include the hydrodynamic damping due to vortices shedding to the wake. In the present work a point load or distributed load replace the $\boldsymbol{L_G}$ forcing terms to calculate the DPM and acoustic pressure. The hydrodynamic damping is negligible because the free-stream velocity is set to zero but the fluid inertia terms M_c are retained. Loss mechanisms (η) include structural-material damping represented by an isotropic, hysteretic loss-factor η through a complex Youngs Modulus $E = E(1 + \mathrm{j}\eta)$ and the acoustic radiation loss factor of the bending motion. The latter is calculated from the radiation resistance: for low-to-medium frequencies an approximate expression of the n^{th} bending mode of a free–free unbaffled beam has been utilized (Blake and Maga, 1975) and for higher frequencies that of a baffled beam is utilized (Lyon and Maidanik, 1962). It is assumed that the loss factor of the torsional vibration is equal to that of the bending vibration. The effect of the viscous damping is not included.

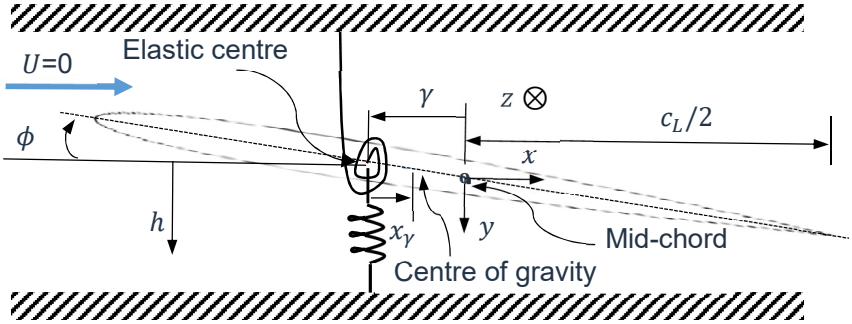

Figure 2 – Geometry of a hydrofoil strip used in the ROM.

The far-field pressure due to the bending vibration of the hydrofoil is calculated from an appropriate frequency-response function for low-to-medium frequencies and from Rayleigh's integral for higher ones (Wallace, 1972). The hydrofoil is discretised into $\alpha = 1, \ldots, M$ chordwise strips along the span (z-direction in Equation 1); applying a finite-difference discretization a $2(M+1) \times 2(M+1)$ linear system of equations $\boldsymbol{A}\hat{\boldsymbol{x}} = \hat{\boldsymbol{b}}$ is obtained. In this system the matrix $\boldsymbol{A}$ is the discretized form of the $\boldsymbol{\mathcal{D}}$ and $\boldsymbol{L_{HP}}$ operators and includes the cantilevered clamped-free boundary conditions, $\hat{\boldsymbol{x}} = \left\{\hat{h}\big|^{\alpha}, \hat{\phi}\big|^{\alpha}\right\}^{T}$ is the vector of unknowns and $\hat{\boldsymbol{b}} = \left[\hat{L}_G^{\alpha}, 0\right]^{\mathrm{T}}$ the forcing vector with the magnitude of the externally applied force per-unit-span at each strip α. The chordwise dependence of the structural vertical-velocity (ξ is the ordinate in the x-direction, $\xi = 0$ at the LE of the hydrofoil) due to the heaving and pitching of the section's elastic centre (see Figure 2) which is utilized for the calculation of the DPM and the acoustic pressure is given by, noting $\gamma c_L/2$ is the position of the elastic centre relative to the mid-chord

$$\hat{u}^{\alpha}(\xi, f) = -\mathrm{j}2\pi f\hat{h}\big|^{\alpha} - \mathrm{j}2\pi f\hat{\phi}\big|^{\alpha}(\xi - (1+\gamma)c_L/2)\,. \tag{2}$$

2.3 Thin-plate theory

We now present a simplified description of the analytical model of Cao et al. (2023) of a clamped-free-free-free (CFFF) thin plate in a fluid. The plate dimensions span L and chord c_L are in the (x, y) plane. The origin of the coordinate system is located at the corner of the plate. The plate is excited by a harmonic point force $f_{(t)}$ located at (x_0, y_0) coordinates. Displacement of any point (x, y) of the plate at time t is denoted by $w(x, y, t)$. The Lagrange function of the plate is $L = KE - PE + U$, in which KE, PE and U are respectively the kinetic energy, potential energy and external work of the plate (Deng et al., 2019). Following Nelisse et al. (1998), the KE determined by

$$KE = \frac{1}{2}\iint_S \rho h(\dot{w})^2 dS \ , \tag{3}$$

where S is the surface area of the plate; PE is calculated as

$$PE = \frac{1}{2}\iint_S B\left[\left(\frac{d^2w}{dx^2}\right)^2 + \left(\frac{d^2w}{dy^2}\right)^2 + 2\nu\frac{d^2w}{dx^2}\frac{d^2w}{dy^2} + 2(1-\nu)\left(\frac{d^2w}{dxdy}\right)^2\right] dS \ , \tag{4}$$

where $B = Eh^3/\left(12(1-\nu^2)\right)$ is the flexural rigidity, E is Young's modulus and ν the Poisson ratio. The work related to the external forces $f(x, y, t)$ acting on the plate, including the point force excitation $f^e(x, y, t)$ and the surface acoustic pressure $f^p(x, y, t)$ due to the fluid loading caused by the plate motion in the fluid, can be expressed by

$$U = \int_S \left(f^e + f^p\right) w \, dS \quad \text{where} \quad f^p = \underbrace{-\lim_{\varepsilon\to 0}\left(P(x, y, t, \varepsilon) - P(x, y, t, -\varepsilon)\right)}_{-\bar{P}(x,y,t)}, \tag{5a,b}$$

in which the function $\bar{P}(x, y, t)$ is called the "pressure jump". The Rayleigh-Ritz method is then used to derive the equations of motion of the plate (Nelisse et al., 1998, Hosseini Hashemi et al., 2010, Dozio, 2011). By expanding $w(x, y, t)$ over basis functions satisfying the plate's boundary conditions, an approximate solution of $w(x, y, t)$ can be found; similarly, the pressure jump $\bar{P}(x, y, t)$, can be written as a set of admissible functions ψ_{mn}. This gives the following forms

$$w(x, y, t) = \sum_{ij} \alpha_{ij}(t)\phi_{ij}(x, y) \quad \text{and} \quad \bar{P}(x, y, t) = \sum_{mn} \bar{P}_{mn}(t)\, \psi_{mn}(x, y) \, . \tag{6a,b}$$

For $w(x, y, t)$, $i = 1, .., M$ and $j = 1, .., N$ in which M and N are the numbers of vibration modes in x and y coordinates respectively; $\phi_{ij}(x, y)$ are the basis functions and $\alpha_{ij}(t)$ are the unknown coefficients. For $\bar{P}(x, y, t)$, $\bar{P}_{mn}$ are unknown pressure coefficients and the functions ψ_{mn} are chosen so that they must vanish on the plate contour with $m = 1, .., M$ and $n = 1, .., N$. Finally, following the same procedure in Nelisse et al. (1998) and assuming that $f(t) = f_0 e^{\mathrm{j}\omega t}$, $\alpha_{ij}(t) = H_{ij}e^{\mathrm{j}\omega t}$ and $\dot{\alpha}_{ij}(t) = \mathrm{j}\omega H_{ij}e^{\mathrm{j}\omega t}$, the final form of the equation of motion is as follows

$$\sum_{pq}\left(K^p_{ijpq} - \omega^2 M^p_{ijpq} + j\omega Z_{ijpq}\right)H_{pq} = f^e_{ij} \, , \tag{7}$$

in which K^p_{ijpq} and M^p_{ijpq} are the stiffness and mass of the plate respectively and Z_{ijpq} is the radiation impedance. Equation 7 is the governing equation of motion of the plate and is used to find the coefficient set H_{pq} for the response of the plate. The displacement of any point of the plate $w(x, y, t)$ is then determined using Equation 6a.

3 RESULTS

The cantilever material is aluminium of density $\rho = 2700\ \mathrm{kg/m^3}$, $E = 70\ \mathrm{GPa}$, $\nu = 1/3$ and loss factor $\eta = 0.01\%$. The fluid is water of density $\rho_f = 1000\ \mathrm{kg/m^3}$ and speed of sound $c = 1500\ \mathrm{m/s}$ @ $26.5°\mathrm{C}$. The system response to the applied force is determined in the frequency range $f = 200\ \mathrm{Hz} - 60\ \mathrm{kHz}$ and wave number when used is calculated as $k = \omega/c = 2\pi f/c$.

Initial numerical simulations were carried out in COMSOL to provide baseline results for the tapered cantilever with NACA0015 aerofoil cross-section. The acoustic radiation (plotted in dB relative to $1 \times 10^{-12}\ \mathrm{W}$) for the various load cases are shown in Figure 3. For low frequencies the difference between the different forcing is relatively much less than for higher frequencies. The low-frequency behaviour is unsurprising as the majority the modes are in bending and the different forcing positions along the chord are still at the same spanwise position. Also as expected the highest noise level is generated when the greatest moment is applied, the TE distributed load response less than that of the TE point load, especially at higher frequencies. Figure 4 shows a typical mode shape at higher frequencies: the majority of the displacement is confined to the TE and hence greater excitation occurs when the load is located at the TE; it is also noted that the same excitation would not occur if equal moment were applied at the LE. Comparing the point load locations, only minor difference is seen between QC and MC point loads. The TE distributed load is only lower than QC and MC point loads in the region of $3\mathrm{kHz}$, this particular phenomena owing to the nature of the tapered beam second and third mode shapes in bending. We can now determine the effectiveness of the ROM to capture the physics demonstrated by the COMSOL model. Figure 5 compares the results of TE point loads using these models on the same tapered cantilever with NACA0015 aerofoil cross-section. Included in the figure for reference is the acoustic radiation of a compact-dipole acoustic-source excited by a concentrated force of amplitude $\hat{F}$ (Ross, 1976)

$$\Pi_f = \omega^2\ \hat{F}^2/\left(12\pi\ \rho_f\ c^3\right). \tag{8}$$

The transition between ROM radiation models for unbaffled and baffled beams occurs at $kc = 4.4$ that for water is $\sim 20\ \mathrm{kHz}$. At low frequency there is good agreement, material damping is too low to compare peak noise. In general we are more interested in comparing one-third octave band (OTOB) levels. At high frequencies the ROM model asymptotes to the radiation of a dipole, under predicting the result from COMSOL. Given the nature of the mode shapes at high frequency shown in the previous section a difference is anticipated: the ROM acoustic radiation is lower as the radiation model only accounts for bending modes, not rotational modes.

An additional reason for lower radiation of the ROM is found when analysing the DPM of the point loads compared to the response at the same location of a distributed load. Figure 6 compares the DPM results of TE point and distributed loads on a uniform plate predicted by COMSOL, ROM and thin-plate models. Hence it is also possible to examine what gain in accuracy can be achieved using a thin-plate model instead of the ROM. We choose a uniform plate as the thin-plate model cannot approximate taper or thickness distribution. This required simplification highlights the versatility of the ROM even though it cannot capture chordwise modes. In Figure 6 also shown are theoretical results for bending of an infinite-beam excited at its centre (Goyder and White, 1980) and a semi-infinite plate excited at its edge (Cremer et al., 2005) that respectively are calculated as

$$\left.\frac{\hat{V}}{\hat{F}}\right|_{\infty} = \frac{(1+i)}{4\rho L c_L\sqrt{\omega}}\left(\frac{\rho L c_L}{B}\right)^{\frac{1}{4}} \quad \text{and} \quad \left.\frac{\hat{V}}{\hat{F}}\right|_{s-\infty} = \frac{1}{3.5\sqrt{B\rho h_{max}}}\ . \tag{9a,b}$$

At low frequency both point load and distributed loads show good agreement. The anti-resonance after the first-mode in bending is much shallower for COMSOL and is caused by the more complex 3D geometry modelled. At high frequency, all point load responses asymptote to that of a semi-infinite plate. For the distributed load, the ROM result asymptotes to that of an infinite beam. However the COMSOL result asymptotes to that of a semi-infinite plate (not shown here). The thin-plate distributed-load asymptotes between these two results, demonstrating an improved capture of the high frequency mode shapes.

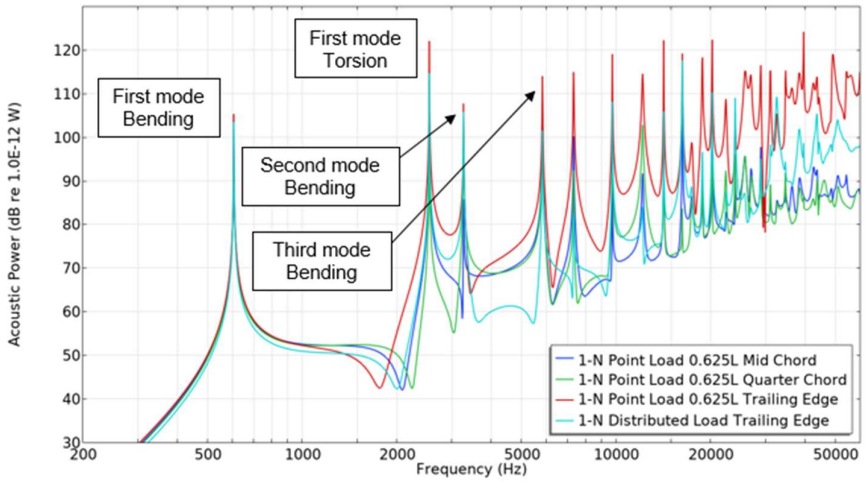

Figure 3 – Acoustic power predictions using COMSOL of water-loaded 50%-tapered NACA0015 cross-section cantilever excited by various loads.

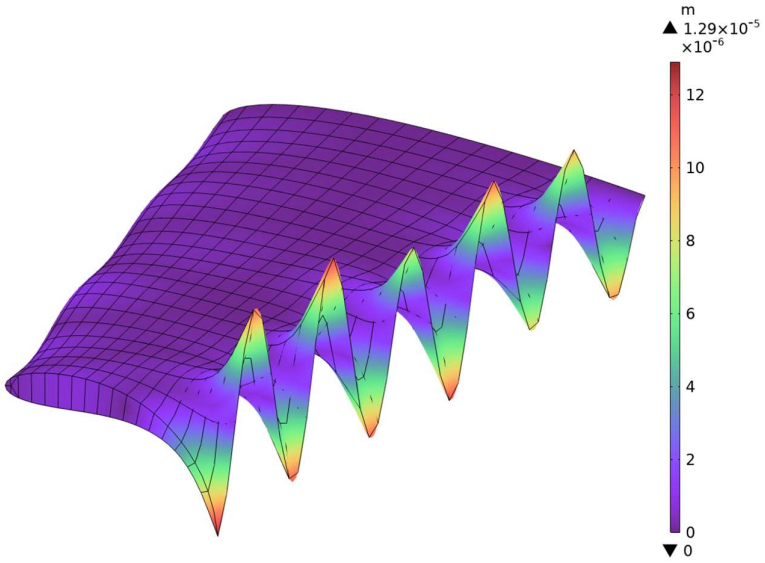

Figure 4 – Operating deflection shape prediction using COMSOL at the peak in acoustic power response at 40 kHz, for the water-loaded 50%-tapered NACA0015 cross-section cantilever.

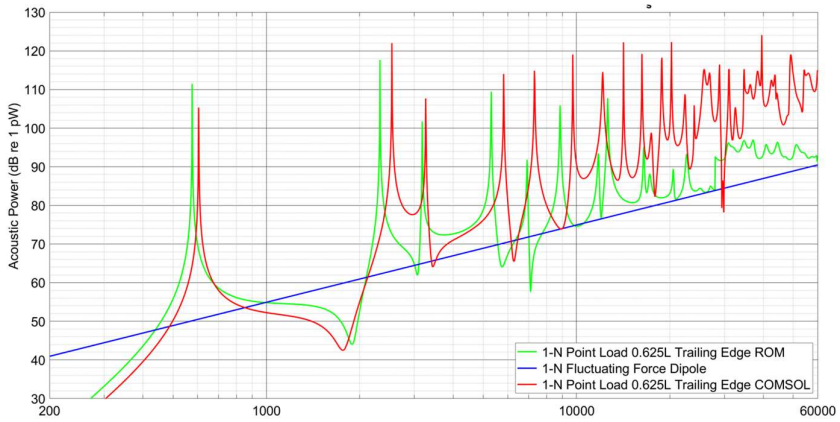

Figure 5 – Acoustic radiated power response of water-loaded cantilevers due to harmonic 1-N point load at the TE, $0.625L$ spanwise location: 50%-tapered NACA0015 cross section cantilever.

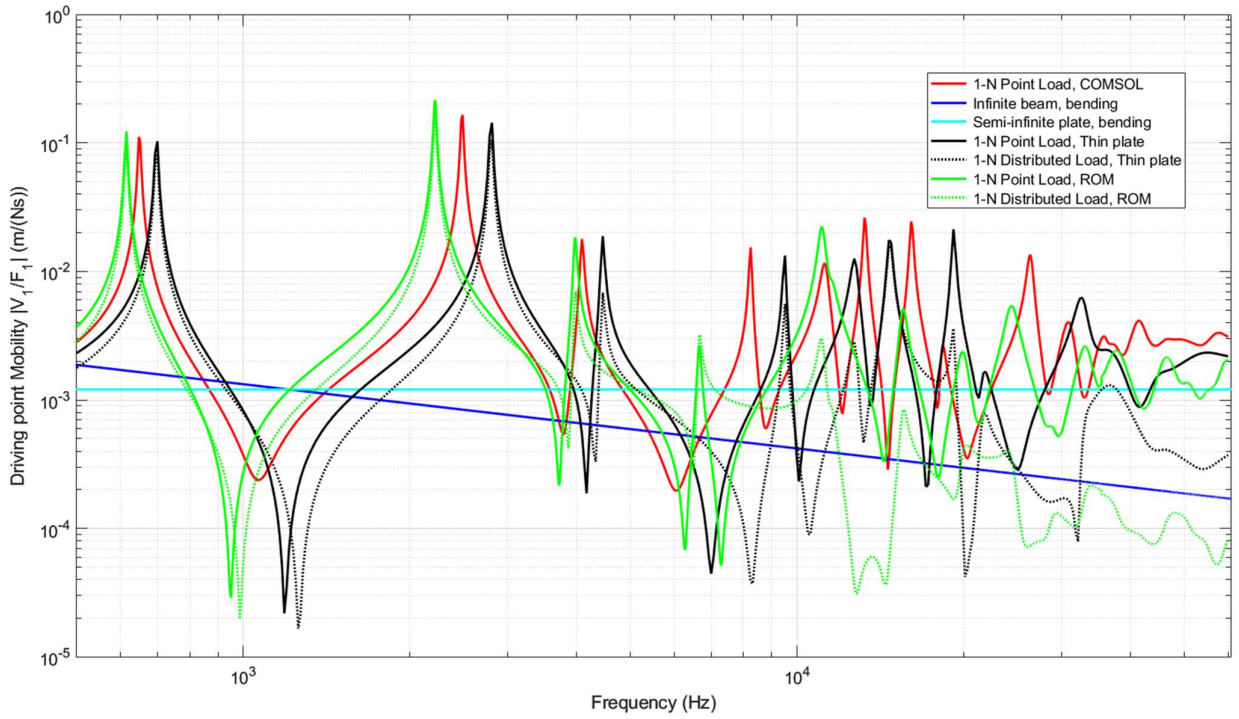

Figure 6 – Drive point mobility of water-loaded cantilevers due to harmonic 1-N point/distributed load at TE, $0.625L$ spanwise location for a uniform plate

4 CONCLUSIONS

This paper has demonstrated the versatility of our ROM to capture the hydroacoustics of complex geometrical plates excited by point or distributed loads. COMSOL was used to give baseline results to compare to. A thin plate model has shown to converge more accurately than the ROM to the COMSOL results for distributed loads at higher frequencies as chordwise mode shapes can be captured. The next stage of development is to calculate the far-field acoustic radiation from the thin plate model; it is noted that the unbaffled method used in the ROM can also be used with the thin plate and gives excellent results (not shown here). An alternative route is to extend another of our 1D models (Howell et al., 2024). to two dimensions by coupling a 2D finite-difference model of a thin plate with a 2D panel method (Lucey and Carpenter, 1993) that imposes the static fluid loading of an ideal fluid. Acoustic radiation would be calculated by coupling with OpenBEM (Henriquez and Juhl, 2010).

REFERENCES

Blake, W. K. and Maga, L. J. (1975). *On the flow−excited vibrations of cantilever struts in water. I. Flow−induced damping and vibration.* The Journal of the Acoustical Society of America **57**(3): 610-625.

Cao, H., Karimi, M., Williams, P. and Dylejko, P. (2023). *Vibration control of a cantilever plate immersed in water using shunted piezoelectric patches.* The Journal of the Acoustical Society of America **154**(4): A55.

Chen, L. and Kessissoglou, N. (2014). *Influence of structural elasticity on trailing edge noise*. INTER-NOISE and NOISE-CON Congress and Conference Proceedings, Melbourne, Institute of Noise Control Engineering.

Cremer, L., Heckl, M. and Petersson, B. (2005). *Structure-Borne Sound: Structural Vibrations and Sound Radiation at Audio Frequencies*, Springer-Verlag.

Deng, J., Zheng, L., Guasch, O., Wu, H., Zeng, P. and Zuo, Y. (2019). *Gaussian expansion for the vibration analysis of plates with multiple acoustic black holes indentations.* Mechanical Systems and Signal Processing **131**: 317-334.

Dozio, L. (2011). *On the use of the Trigonometric Ritz method for general vibration analysis of rectangular Kirchhoff plates.* Thin-Walled Struct. **49**(1): 129-144.

Goyder, H. G. D. and White, R. G. (1980). *Vibrational power flow from machines into built-up structures, part I: introduction and approximate analyses of beam and plate-like foundations.* Journal of Sound and Vibration **68**(1): 59-75.

Henriquez, V. C. and Juhl, P. M. (2010). *OpenBEM-an open source boundary element method software in acoustics.* Internoise 2010 **7**: 5796-5805.

Hosseini Hashemi, S., Karimi, M. and Rokni Damavandi Taher, H. (2010). *Vibration analysis of rectangular Mindlin plates on elastic foundations and vertically in contact with stationary fluid by the Ritz method.* Ocean Engineering **37**(2): 174-185.

Howe, M. (1993). *The compact Green's function for a semi-infinite elastic plate, with application to trailing edge noise and blade–vortex interaction noise.* The Journal of the Acoustical Society of America **94**(4): 2353-2364.

Howell, R. M., Croaker, P., Dylejko, P., Gargan-Shingles, C. and Skvortsov, A. (2022). *Estimating propeller trailing-edge pressure using the BPM method*. Proceedings of the Acoustics Australia Conference.

Howell, R. M., Lucey, A. D., Tsigklifis, K., Dylejko, P. and Ng, T. (2024). *A new model for crossflow fluid-structure instabilities of helicopter blades.* Proceedings of Meetings on Acoustics **52**(1).

Lucey, A. D. and Carpenter, P. W. (1993). *The hydroelastic stability of three-dimensional disturbances of a finite compliant wall.* Journal of Sound and Vibration **165**(3): 527-552.

Lyon, R. H. and Maidanik, G. (1962). *Power flow between linearly coupled oscillators.* The Journal of the Acoustical Society of America **34**(5): 623-639.

Nelisse, H., Beslin, O. and Nicolas, J. (1998). *A generalized approach for the acoustic radiation from a baffled or unbaffled plate with arbitrary boundary conditions, immersed in a light or heavy fluid.* Journal of Sound and Vibration **211**(2): 207-225.

Peters, H., Chen, L. and Kessissoglou, N. (2014). *The effect of flow on the natural frequencies of a flexible plate*. INTER-NOISE and NOISE-CON Congress and Conference Proceedings, Melbourne, Institute of Noise Control Engineering.

Ross, D. (1976). *Mechanics of Underwater Noise*. New York, Pergamon Press.

Smith, S. M., Brandner, P. A., Pearce, B. W., Venning, J. A., Moreau, D. J. and Clarke, D. B. (2021). *Steady and unsteady loading on a hydrofoil immersed in a turbulent boundary layer.* Journal of Fluids and Structures **102**: 103225.

Tsigklifis, K., Wong, M., De Candia, S., Dylejko, P., Croaker, P. and Skvortsov, A. (2021). *Reduced order modelling of vibroelastic response of a hydrofoil in homogeneous isotropic turbulence*. Proceedings of Acoustics Australia Conference, Woolongong.

Tsigklifis, K., Wong, M., Dylejko, P., McGillivray, I. and Howell, R. (2022). *Validation of the vibroacoustic model of a propeller with elastic blades*. DST Technical Report.

Tsigklifis, K., Wong, M., Dylejko, P., Karimi, M., Croaker, P. and Skvortsov, A. (2024). *Reduced-order modelling of flow-induced vibration from turbulence impingement*. Flinovia IV, Sydney.

Wallace, C. (1972). *Radiation resistance of a rectangular panel.* The Journal of the Acoustical Society of America **51**(3B): 946-952.

Wong, M., Tsigklifis, K., Dylejko, P., Karimi, M., Croaker, P. and Skvortsov, A. (2022). *Estimating the Vibration Response of a Hydrofoil in Homogeneous Isotropic Turbulence Using the Uncorrelated Wall Plane Wave*. 23rd Australasian Fluid Mechanics Conference, Sydney.